

## Seasonal dynamics of the near-surface alongshore flow off central Chile

Catalina Aguirre,<sup>1</sup> Óscar Pizarro,<sup>2</sup> Paul T. Strub,<sup>3</sup> René Garreaud,<sup>1</sup> and John A. Barth<sup>3</sup>

Received 13 June 2011; revised 3 November 2011; accepted 6 November 2011; published 7 January 2012.

[1] The seasonal cycle of the near-surface circulation off central Chile was analyzed using satellite altimetry and an oceanic model. To evaluate the role of the wind stress curl on the circulation we performed two identical simulations except for the wind-forcing: the “control run” used long-term monthly mean wind stress and the “no-curl run” used a similar wind stress field, but without curl. The observed and modeled (control run) surface currents showed a strong seasonal cycle and a well-defined equatorward flow with a jet like-structure. This jet develops during spring and summer, consistent with the presence of a low-level wind jet. South of Punta Lavapie cape ( $\sim 37^\circ\text{S}$ ), the equatorward surface current remains close to the coast. After the flow-passes this cape, however, it separates to become an offshore jet. In contrast, in the no-curl simulation the separation at Punta Lavapie is not observed and the offshore jet farther north is not present, demonstrating the importance of the wind stress curl on the dynamics of this flow. Although the offshore integrated Sverdrup transport was similar to the model transport, the offshore jet was not located where the wind stress curl was maximum. Instead, the position of the jet followed approximately the zero wind stress curl, which corresponds to the climatological location of the low-level wind jet axis. These results illustrate the importance of the offshore upwelling/downwelling associated with curl-driven Ekman pumping, which tilts isopycnals upward (downward) toward the east (west) of the wind jet, forcing a northward flow through thermal wind balance.

**Citation:** Aguirre, C., Ó. Pizarro, P. T. Strub, R. Garreaud, and J. A. Barth (2012), Seasonal dynamics of the near-surface alongshore flow off central Chile, *J. Geophys. Res.*, *117*, C01006, doi:10.1029/2011JC007379.

### 1. Introduction

[2] Major eastern boundary current systems are driven by predominant equatorward winds, which force upwelling of cold subsurface water near the coast, equatorward surface flows with a complex spatial and temporal structure, and a poleward undercurrent [e.g., Hill *et al.*, 1998]. Seasonal changes in the wind field modulate the upwelling variability and the different surface and subsurface flows observed in these regions [Strub *et al.*, 1998]. In the vast region comprising the Chile-Peru Current System, the seasonal cycle of the wind shows contrasts between its northern and southern portions. In the northern region off Peru ( $\sim 5^\circ\text{S}$ – $15^\circ\text{S}$ ) winds are upwelling favorable all year-round with maximum speeds in the austral winter (June, July and August; JJA). Off northern Chile ( $\sim 18^\circ\text{S}$ – $28^\circ\text{S}$ ) upwelling winds also prevail throughout the year, but they are rather weak and stable, with very low synoptic and seasonal variability

[Pizarro *et al.*, 1994]. In contrast, off central Chile ( $\sim 30^\circ\text{S}$ – $40^\circ\text{S}$ ) winds show a large seasonal cycle [e.g., Garreaud and Muñoz, 2005]. During austral winter, the Southeast Pacific Anticyclone and the westerly wind belt move northward, allowing the arrival of midlatitude atmospheric disturbances to central Chile as far north as  $\sim 30^\circ\text{S}$ , which increase the frequency and magnitude of poleward winds [e.g., Fuenzalida, 1971; Saavedra and Foppiano, 1992]. Indeed, south of  $\sim 35^\circ\text{S}$  mean coastal winds are downwelling favorable during winter. During summer (December, January and February; DJF), the Southeast Pacific Anticyclone moves southward and upwelling winds are predominant down to  $\sim 40^\circ\text{S}$ . In this season, a synoptic low-level wind jet blowing northward is frequently observed between  $\sim 38^\circ\text{S}$  and  $30^\circ\text{S}$  [Garreaud and Muñoz, 2005].

[3] The presence of the wind jet leads to a consideration of the role of wind stress curl in causing upwelling. In the offshore region, the wind stress curl field off central Chile is mostly anticyclonic (downwelling favorable). The coastal band is dominated by cyclonic (upwelling favorable) curl, which exhibits a distinct annual cycle [Bakun and Nelson, 1991]. In summer, when the equatorward wind stress is more intense, stronger cyclonic (anticyclonic) wind stress curl develops east (west) of the wind jet axis, commonly located at about 150 km offshore [Garreaud and Muñoz, 2005]. This low-level wind jet and the associated wind

<sup>1</sup>Department of Geophysics, University of Chile, Santiago, Chile.

<sup>2</sup>Department of Geophysics and COPAS, University of Concepcion, Concepcion, Chile.

<sup>3</sup>College of Oceanic and Atmospheric Sciences, Oregon State University, Corvallis, Oregon, USA.

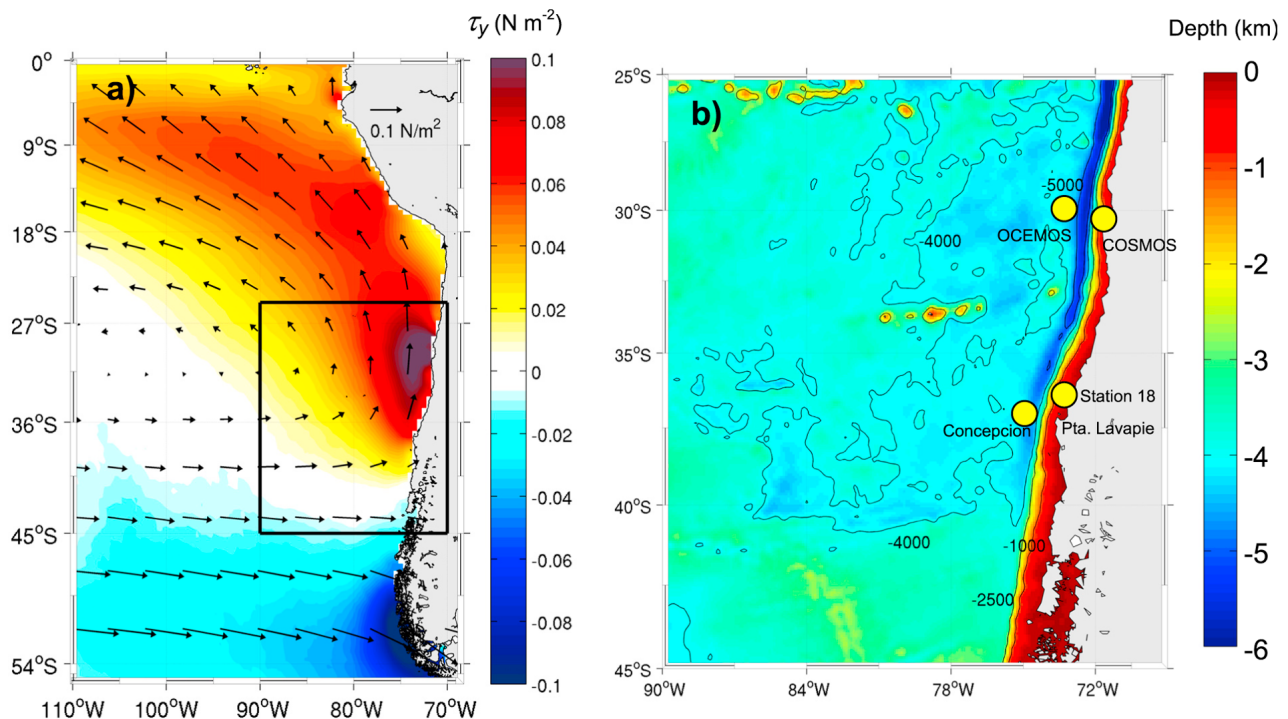


**Figure 1.** (a) Mean of the meridional wind stress magnitudes (colors,  $\text{N m}^{-2}$ ) and wind stress vectors (arrows) derived from QuikSCAT satellite data for the period 2000–2007. The black square indicates the model domain used in this study. (b) Bottom topography of the study area obtained from the ETOPO2 data set. Depth contours are shown for 1000 m, 2500 m, 4000 m and 5000 m. In addition, yellow dots indicate the mooring locations.

stress curl may play a major role in coastal upwelling dynamics and surface circulation off central Chile, one focus of this paper.

[4] The main features of the upper-ocean regional circulation in the eastern South Pacific have been extensively reviewed by *Strub et al.* [1998]. They identified four major currents off central Chile: (1) the Chile-Peru Current (also known as the Humboldt Current), which is the surface equatorward flow traditionally identified as the eastern branch of the subtropical South Pacific gyre; (2) a coastal jet called the Chile Coastal Current that flows equatorward and is directly related to the upwelling dynamics; (3) the Peru-Chile Countercurrent, which is a surface poleward flow located farther west of the Chile Coastal Current, about 100–300 km offshore [*Strub et al.*, 1995] and (4) the Peru-Chile Undercurrent, which is a coherent subsurface current that flows poleward over the slope along the Peruvian and Chilean coasts [e.g., *Silva and Neshyba*, 1979; *Huyer et al.*, 1991a; *Shaffer et al.*, 1997]. Based on satellite-tracked, near-surface (15 m depth) drifters, *Chaigneau and Pizarro* [2005] observed a mean surface equatorward flow extending offshore to about 82°W off central Chile, with a mean speed of about  $6 \text{ cm s}^{-1}$ . This flow is consistent with the large-scale South Pacific gyre circulation, traditionally recognized by classical geostrophic calculations based on hydrographic data. However, using satellite-derived surface geostrophic currents, *Fuenzalida et al.* [2008] described a jet-like stream as a central component of the Chile-Peru Current, with a summer intensification. By analyzing satellite winds they suggest that this jet is related to the seasonal

increase of the anticyclonic wind stress curl by means of Sverdrup dynamics.

[5] Only a few studies have addressed the dynamics of the regional ocean circulation and its seasonal variability off Chile. The few numerical modeling studies have focused on the intense upwelling region near 37°S [*Batteen et al.*, 1995; *Leth and Shaffer*, 2001; *Leth and Middleton*, 2004; *Mesias et al.*, 2001, 2003], where the oceanic jet observed farther north seems to begin. These simulations have shown a surface coastal jet, which separates from the coast around Punta Lavapie ( $\sim 37^\circ\text{S}$ , Figure 1b), creating a meander that gives rise to a large upwelling plume north of 36°S. This jet and its separation have been recently confirmed by satellite and hydrographic data [*Letelier et al.*, 2009]. These results suggest that the jet observed in the coastal transition zone (CTZ), about 100–200 km offshore off central Chile during the upwelling season (usually from November to March), is related to a current that detaches from the coast at Punta Lavapie. This jet may play a major role in the surface circulation off Central Chile, but its dynamics and seasonal variability remain almost unknown.

[6] Here we use the Regional Ocean Modeling System (ROMS) along with surface geostrophic currents, derived from satellite altimetry, and QuikSCAT winds to analyze the circulation off central Chile ( $\sim 25^\circ\text{S}$ – $45^\circ\text{S}$ ). The main focus of the paper is on the jet observed in the CTZ off central Chile during spring and summer. We particularly address the effects of the seasonal variability of the wind stress and the wind stress curl on the surface alongshore currents.

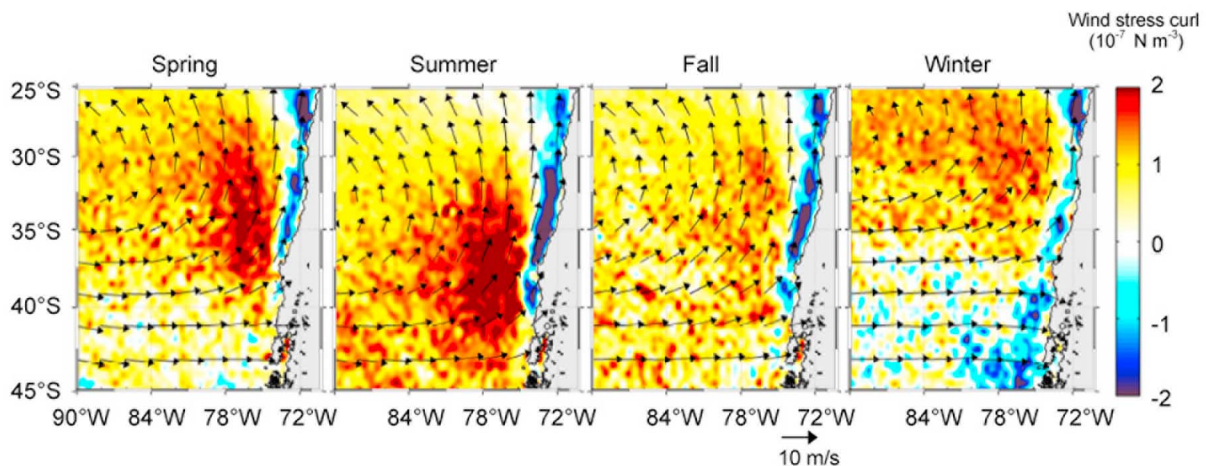


**Figure 2.** Mean wind velocity (vectors) and wind stress curl (colors,  $10^{-7} \text{ N m}^{-2}$ ) off central Chile derived from QuikSCAT satellite data for the period 2000–2007.

[7] The rest of the paper is organized as follows: in section 2 we describe the satellite observations and the numerical model used in this study. The main results are presented in section 3, in which we first present the model validation and then address the seasonal variability of the upwelling and surface currents. This is followed by an analysis of the vertical structure of the major surface currents produced by the model. Finally, we analyze the role of the wind stress curl on surface circulation, particularly on the position and intensity of the CTZ jet, through a comparison with a second simulation which lacks the wind stress curl forcing. The main results are discussed in section 4 and conclusions are summarized in section 5.

## 2. Observations, Methods and Model

### 2.1. Data Sets and Data Processing

[8] We focus on a large region covering central Chile between  $25^{\circ}\text{S}$ – $45^{\circ}\text{S}$  and extending from the coast to  $90^{\circ}\text{W}$  (Figure 1a). We use sea level anomalies (SLA) and geostrophic surface current anomalies derived from altimetry from 1993 to 2007. Maps in a Mercator grid of  $1/3^{\circ}$  spatial resolution are derived by SSALTO/DUACS and distributed by AVISO (Archiving, Validation, and Interpretation of Satellite Oceanographic data). Time series with weekly temporal resolution are monthly averaged. The absolute surface velocity is obtained by adding a mean geostrophic current based on the dynamic height estimated using temperature and salinity climatologies from CARS (CSIRO Atlas of Regional Seas) 2006 [Ridgway *et al.*, 2002] with 1000 db as the reference level. We use wind stress from QuikSCAT data from 2000 to 2007. Monthly mean wind stress data with a spatial resolution of  $0.5^{\circ}$  are obtained from Centre d’Exploitation et de Recherche Satellitaire d’Archivage et de Traitement (CERSAT), at Institut Francais de Recherche pour l’Exploitation de la Mer (IFREMER). The seasonal cycles of the wind stress and wind stress curl based on these data are presented in Figure 2.

[9] The wind data allow us to compare the relative contributions of the Ekman transport and Ekman pumping to the

vertical velocities and transports near the coast. The Ekman pumping vertical velocities ( $w$ ) are estimated directly from the curl of the wind stress ( $\bar{\tau}$ ) fields [e.g., Stewart, 2008]

$$w = \nabla \times \frac{\bar{\tau}}{\rho f}, \quad (1)$$

where  $\rho$  is a typical density for seawater ( $1025 \text{ kg m}^{-3}$ ) and  $f$  is the Coriolis parameter. These vertical velocities are then integrated from the coast to  $\sim 150 \text{ km}$  and in each  $0.5^{\circ}$  of latitude to obtain the vertical transports. The Ekman transport near the coast is estimated by

$$M = \frac{\tau_y}{\rho f}, \quad (2)$$

where  $\tau_y$  is the alongshore (assumed meridional in the study region, positive to the north) component of wind stress. These values are also integrated every  $0.5^{\circ}$  of latitude. In this case we only integrated meridionally, considering that the offshore Ekman transport  $M$  ( $\text{m}^2 \text{ s}^{-1}$ ) is completely compensated by a vertical transport near the coast.

[10] To evaluate the quality of the variability of the velocities estimated from the gridded altimetry and the model, in situ currents measurements are used (Table 1). Hourly data were obtained from four moorings located off  $\sim 30^{\circ}\text{S}$  and  $\sim 37^{\circ}\text{S}$  (Figure 1b). Two moorings were located close to the coast, about 13 km offshore at  $30^{\circ}\text{S}$  (COSMOS) and about 20 km offshore at  $37^{\circ}\text{S}$  (Station 18). Both moorings were instrumented with a 300 kHz acoustic Doppler current profiler (ADCP) pointing upward. In addition, four recording current meters (RCM 7) are available at  $30^{\circ}\text{S}$ . Because the observed vertical structure of currents is more clearly defined in coastal regions than in offshore areas, these coastal data are used to validate the model velocities profiles. The other two moorings are farther offshore ( $>100 \text{ km}$ ) and are used to compare upper-ocean current variability with the satellite data. At  $37^{\circ}\text{S}$  the mooring was instrumented with an ADCP (Concepción), but we only use the measurements at 50 m depth. At  $30^{\circ}\text{S}$  the shallowest measurement is from a RCM 7 located at 340 m depth

**Table 1.** Information About the Moorings and Measurements

Site	Instrument	Latitude	Longitude	Start Time	End Time	Instrument Depth Measurement (m)	Water Depth (m)
OCEMOS	RCM7	30°00'S	73°15'W	Jan 1996	Sep 2006	340	4400
COSMOS	ADCP	30°21'S	71°47'W	Apr 2003	Sep 2006	10–110 (bin 5 m)	950
	RCM7			Nov 1991	Sep 2008	220	
	RCM7			Sep 2000	Oct 2003	330	
	RCM7			Nov 1991	Apr 2009	480	
	RCM7			Nov 1991	Jun 2008	750	
Concepción Station 18	ADCP	37°03'S	74°50'W	Nov 2003	Oct 2006	50	4600
	ADCP	36°28'S	73°10'W	Jan 2009	Jan 2011	6–86 (bin 4 m)	100

(OCEMOS). Table 1 lists the positions, start and end times of the current meter records, and the depth of the water column. The squared coherence values between the satellite-derived geostrophic velocities and the in situ offshore currents are plotted in Figure 3. Despite the fact that the satellite-derived geostrophic currents represent surface velocities and the in situ data are from 50 and 340 m depth, they show significant coherence at periods longer than 100 days. The phase is close to zero at these periods. The use of rotary spectra is preferred because oceanic velocity vectors do not present a dominant direction.

[11] To validate the seasonal cycle of modeled sea level, in situ data near the coast registered by tide-gauges at four different locations are analyzed. These data were provided by the Servicio Hidrográfico y Oceanográfico de la Armada (SHOA), and they are from Caldera (27.1°S–70.8°W), Coquimbo (30°S–71.4°W), Valparaíso (33°S–71.6°W) and Talcahuano (36.7°S–73.1°W).

## 2.2. Model and Model Setup

[12] The model used in this research is the Regional Oceanic Modeling System, which is a split-explicit, free

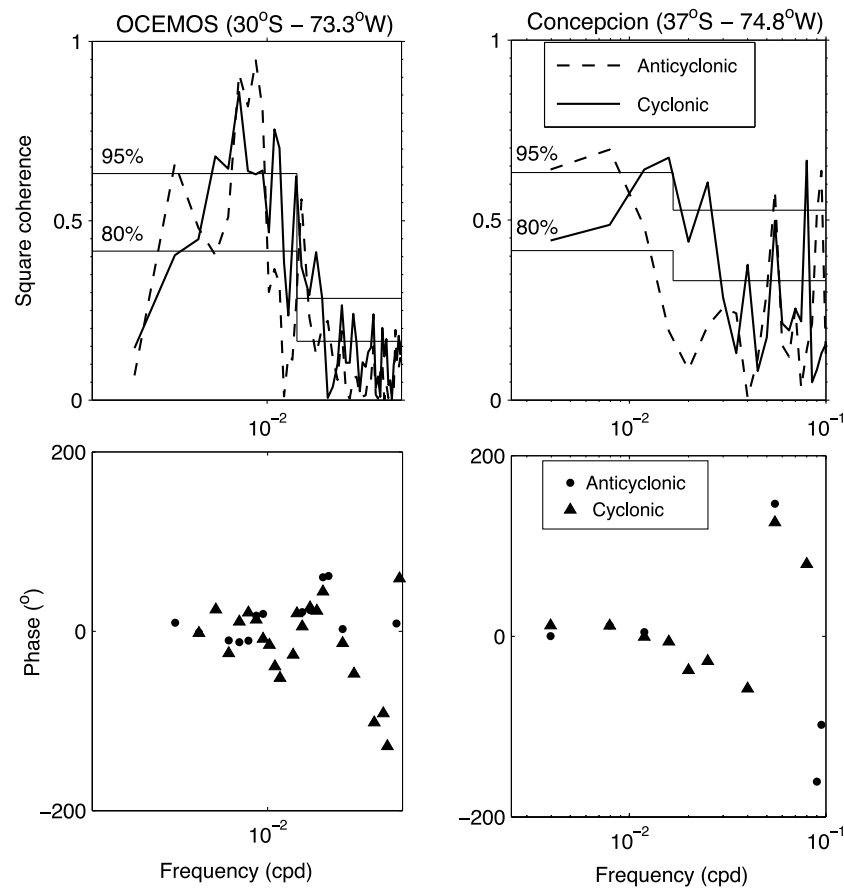


**Figure 3.** (top) Rotary coherence and (bottom) phase between the cyclonic and anticyclonic components of the satellite-derived surface current anomalies (AVISO) and in situ observations at OCEMOS ( $\sim 30^{\circ}\text{S}$ – $73.3^{\circ}\text{W}$ ) and Concepción ( $\sim 37^{\circ}\text{S}$ – $78.4^{\circ}\text{W}$ ). Horizontal lines indicate 80% and 95% coherence significance levels. Phase results for values higher than 80% are plotted for the cyclonic (triangles) and anticyclonic (dots) components. The depths of the in situ currents are 340 m at  $30^{\circ}\text{S}$  and 50 m at  $37^{\circ}\text{S}$ .

surface, topographically following-coordinates oceanic model [Shchepetkin and McWilliams, 2005]. ROMS solves the primitive-equations in hydrostatic and incompressible conditions. Where boundaries are open, oblique radiation conditions are used to estimate the direction of information flux in order to treat the inward and outward fluxes of information separately. When information fluxes are outward the boundary is passive and when they are inward the boundary is active [Marchesiello *et al.*, 2001]. In order to absorb disturbances and reduce noise associated with the radiation condition, the model uses a sponge layer, which is a region of increased horizontal viscosity close to the open boundaries. In our simulations we use a 50 km wide sponge layer. The vertical mixing is parameterized using the K-Profile Parameterization (KPP), which is a non-local closure scheme based on the boundary layer formulation by Large *et al.* [1994].

[13] We carried out a climatological simulation (control run) off central Chile (between 25°S–45°S and 70°W–90°W) with a horizontal resolution of 1/10° (between 7.9 and 10.1 km) and 32 sigma levels in the vertical. We used long-term monthly means from 8 years of QuikSCAT data (2000–2007) as surface boundary conditions of wind stress and Comprehensive Ocean-Atmosphere Data Set (COADS) climatology to calculate the surface heat and freshwater fluxes [da Silva *et al.*, 1994]. The initial and lateral boundary conditions were obtained from the World Ocean Atlas 2005 monthly climatology [Locarnini *et al.*, 2006; Antonov *et al.*, 2006]. The model topography (Figure 1b) is based on the global ETOPO2 at 2' resolution [Smith and Sandwell, 1997]. The model runs for 10 years of 360 days with a spin up period of 2 years, so model climatology was based on the last 8 years. All the output variables were daily averaged. Geostrophic surface currents were calculated using the model sea level ( $\eta$ ) to better compare with satellite-derived surface currents.

[14] To understand the role of the wind stress curl in the formation of the CTZ jet we performed a second simulation, identical to the control run except that the wind stress forcing did not have curl (no-curl simulation). The wind stress field only has the meridional component ( $\tau_x = 0$  everywhere), which retains the observed latitudinal variation but it is constant in longitude. At each latitude, the modified wind stress is estimated by averaging the meridional component of the wind stress between the coast and 80°W.

### 3. Results

#### 3.1. Model Validation

[15] We use satellite and in situ data to validate the model outputs and we contrast the model near-surface circulation with known features of the Chile-Peru Current System.

[16] The seasonal mean of the simulated and satellite SLA are compared, but it is important to note that a climatological simulation lacks the energetics of intraseasonal and interannual forcing. This last may modulate the amplitude of the seasonal scale variability. Although the altimeter data exhibits larger seasonal amplitude, the modeled and observed SLA are similar in their patterns (Figure 4). Low (high) anomalies are generated in a narrow strip close to the coast during summer (winter), consistent with the seasonal variability of the wind stress. Offshore, the simulated SLA show

more structures with relatively smaller scales than those observed in the altimetry data, which is smoothed in the process of creating gridded fields from multiple altimeters. To validate the model seasonal variability near the coast, we compared the model coastal sea level with tide-gauges data at four different locations (Figure 5). Model sea level agrees well with the in situ observations, including the fact that the annual cycle is larger at Talcahuano (~36.6°S).

[17] The vertical sections of the alongshore (meridional) currents at latitudes of 30°S and 36°S (Figures 6a and 6c) are consistent with the major currents of the Southeast Pacific as identified by Strub *et al.* [1998]. Near the coast, within the first ~50 km, the model reproduces an equatorward jet that represents the Chile Coastal Current (CCC). At 30°S the CCC is stable and is present year-round; it only slightly weakens during fall (not shown). Over the continental slope, below the CCC, the model exhibits a poleward flow that is consistent with the Peru-Chile Undercurrent (PCU). At 30°S, this current is observed during the whole year, with maximum values of ~15 cm s<sup>-1</sup> near its core, which is located between 150 and 300 m depth. This mean value agrees well with the annual mean value of 13 cm s<sup>-1</sup> obtained for a 6 year period of current measurements near the PCU core over the slope at 30°S [Shaffer *et al.*, 1999].

[18] Another poleward flow is observed farther offshore, between 150 and 200 km from the coast, extending from surface to more than 500 m north of ~33°S. This flow can be associated with the Peru-Chile Countercurrent (PCCC). The PCCC may be clearly differentiated from the PCU north of ~33°S. In contrast, at 36°S the poleward flow that reaches the surface west of the CCC, may be associated with an outcrop of the PCU more than the PCCC. Penven *et al.* [2005] found that the PCCC appears indiscernible from the PCU at lower latitudes (6°S–10°S) and that the PCU outcrops at about 100 km from the shore at southern latitudes (10°S–20°S). These results seem to be consistent with those obtained using a linear model by McCreary and Chao [1985], who argued that the undercurrent may reach the surface in the case of cyclonic stress curl. Therefore, Penven *et al.* speculated that the currents observed by Strub *et al.* [1995] in 3 years of altimeter data and identified as the PCCC might correspond to the outcropping of the PCU. Nevertheless, in our model fields north of ~33°S, the PCCC is clearly different than the PCU and flows poleward offshore of the CCC and onshore of the Chile-Peru Current (CPC), in agreement with the location described by Strub *et al.* [1995]. The CTZ jet's seasonality, origin, structure, transports and dynamics, as key components of the CPC, are the focus of this paper. A validation of the surface currents of this flow using altimetry data is part of the next section.

[19] Further verification of the model performance in simulating the mean currents is provided in Figures 6b and 6d by the mean vertical profiles of zonal ( $u$ ) and meridional ( $v$ ) velocity components, along with their observational counterparts from two moorings at COSMOS and Station 18 (Table 1). Mean profiles from model and observations are very similar, their shapes agree well and the model captures the reversal of the currents at different depths. At COSMOS, the model profiles show an overestimation of the northward surface current, but the intensity of the PCU at 220 m depth is well represented by the model with values around 15 cm s<sup>-1</sup>.

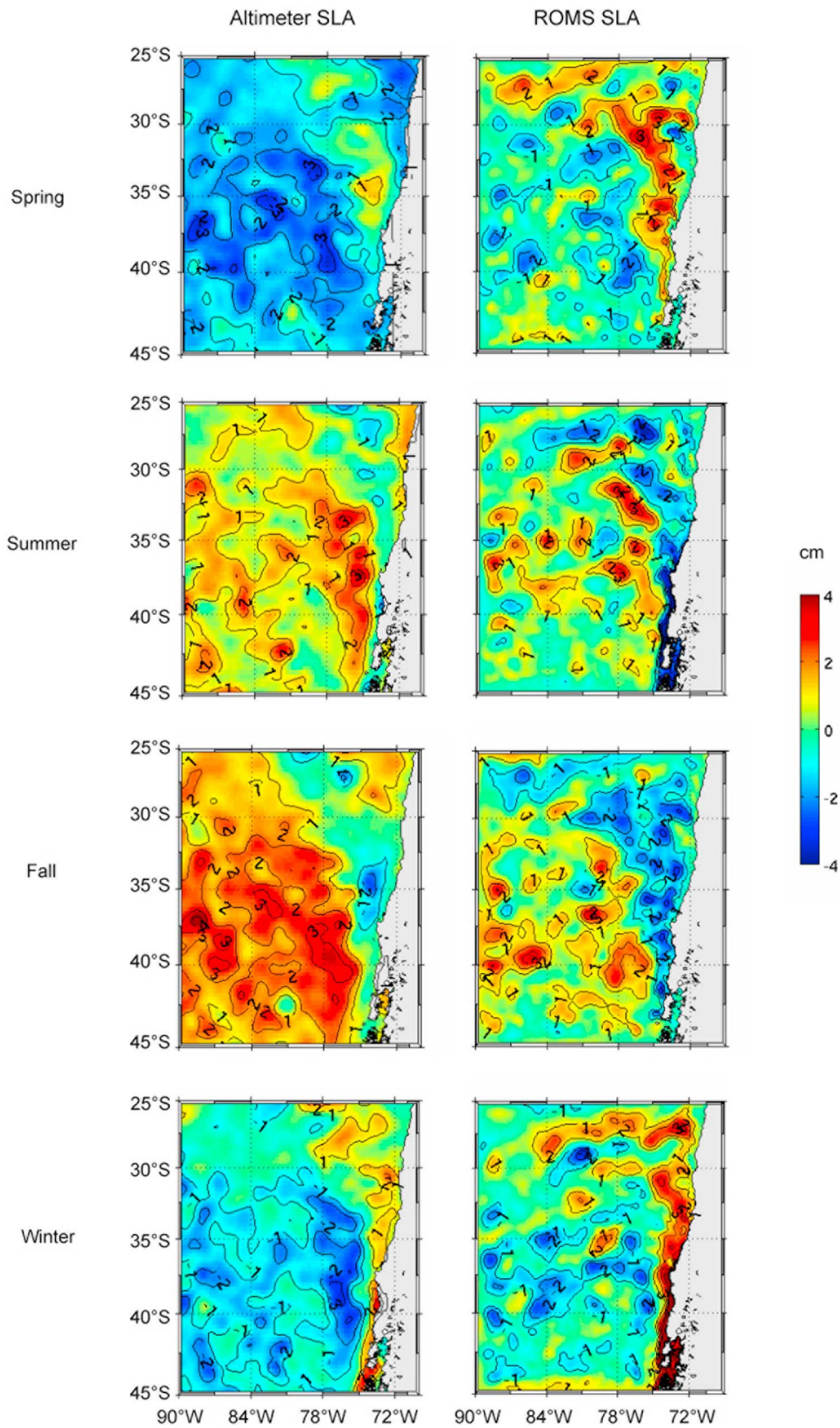


**Figure 4.** Seasonal climatology of the sea level anomalies (SLA) obtained (left) from AVISO altimetry and (right) from ROMS sea level data.

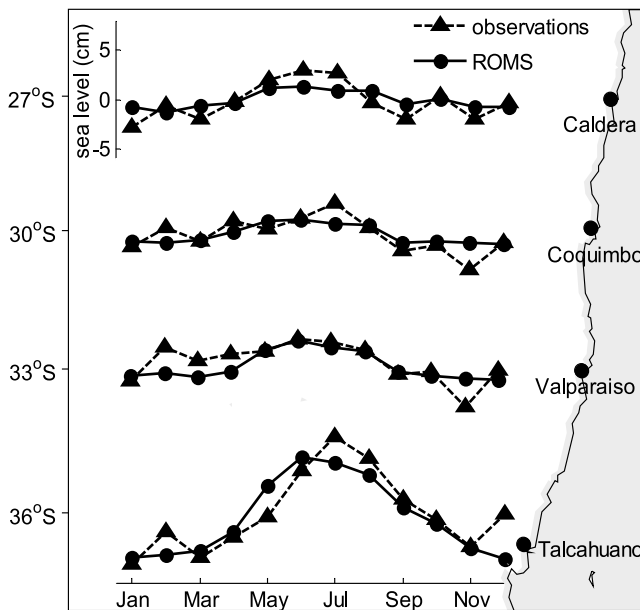


**Figure 5.** Seasonal sea level at the coast in Caldera (27.1°S–70.8°W), Coquimbo (30°S–71.4°W), Valparaíso (33°S–71.6°W) and Talcahuano (36.7°S–73.1°W) obtained from tide gauges and the simulated sea level approximately 4 km offshore.

### 3.2. Seasonal Variability of the Upwelling and Surface Currents

[20] Near the Chilean coast north of 36°S, both the offshore Ekman transport and the Ekman pumping due to the wind stress curl are predominantly upwelling favorable (Figures 7a and 7b; see also Figure 2). South of 36°S, poleward wind stress induces downwelling during winter. Slight downwelling is also induced by the anticyclonic wind stress curl near 38°S during much of the winter and spring. Vertical transport associated with Ekman transport is about one order of magnitude larger than the transport related to Ekman pumping in most of the region. But during summer, between 32°S and 37°S, the low level atmospheric jet centered around 150 km offshore reaches maximum intensities and the Ekman pumping is also intensified, reaching about one half of the Ekman transport. Figure 7d shows the vertical transport near the coast integrated between 27°S and 40°S, and the vertical transport obtained from the ROMS model. Model vertical transport agrees well with the vertical transport estimated from the Ekman transport plus Ekman pumping, with a maximum value of  $\sim 1.7$  Sverdrup (Sv) during summer and a minimum of  $\sim 0.6$  Sv in winter. If we consider the total wind-driven upwelling, model values are slightly lower (higher) than those estimated from the satellite wind stress during the first (second) half of the year. Note that model vertical velocities may also be affected by other mechanisms, particularly by mesoscale eddies, which become important south of 30°S [e.g., Hormazabal *et al.*, 2004]. Nevertheless, those values should tend to vanish when we integrate in a large area that may include cyclonic and anticyclonic eddies.

[21] These results show that Ekman transport is the main mechanism forcing coastal upwelling since Ekman pumping,

related to the wind stress curl, is always much smaller off central Chile. Nevertheless we are probably underestimating the wind stress curl due to the resolution of QuikSCAT data, in particular near the coast, where the curl is negative (upwelling favorable). In fact, Capet *et al.* [2004] infer that present wind analyses do not adequately represent the speed drop-off near the coast. Specifically, off central Chile the cross-shore wind gradient may be large due to the low-level atmospheric jet observed during upwelling seasons [cf., Muñoz and Garreaud, 2005]. Differences in the wind stress curl near the coast may also influence the coastal circulation [Capet *et al.*, 2004].

[22] The surface geostrophic flow estimated from both satellite altimetry and model sea level shows a well defined equatorward current with a jet like-structure during spring and summer (Figures 8a and 8b). The jet remains close to the coast south of Punta Lavapie ( $\sim 37^\circ$ S) with velocities larger than  $10 \text{ cm s}^{-1}$ . North of Punta Lavapie, the coast changes its orientation and the jet separates from the coast. Farther north, during summer, the jet bends to the northwest at around 30°S, remaining over the deep ocean. During fall the jet is still observed, but it is located farther offshore, with a core west of 75°W, between 35°S and 39°S. In contrast, during winter the equatorward flow is much weaker and disorganized, and a poleward flow develops close to the coast in the southern region, consistent with the predominant poleward wind stress found there (Figure 2).

[23] The model reproduces reasonably well the coastal jet in the southern part of the domain and very importantly, the jet separation observed at Punta Lavapie ( $\sim 37^\circ$ S), which subsequently forms the CTZ equatorward flow centered at 75°W (Figure 8b). Nevertheless, model velocities show more spatial structure than observations and larger values than that estimated from satellite altimetry. In addition, the model exhibits an intense coastal equatorward jet year-round within a narrow coastal strip ( $\sim 40$  km), which cannot be compared using satellite-derived geostrophic currents. During summer the model exhibits a surface poleward flow east of the CTZ jet (between 27°S and 33°S) consistent with the PCCC, which was also suggested by 3 years of satellite-derived currents anomalies [Strub *et al.*, 1995], although it is not clearly distinguished in our longer record of surface geostrophic current (Figure 8a).

[24] The jet-like stream observed during summer was originally described by Fuenzalida *et al.* [2008] using maps of absolute dynamical topography combining satellite sea level height anomalies and mean ocean dynamic topography. They indicate that maximum values of the geostrophic velocities do not exceed  $10 \text{ cm s}^{-1}$ . In our case, we used a different ocean dynamic topography, but maximum equatorward speeds are similar to those found by Fuenzalida *et al.* [2008]. Equatorward speeds rarely exceed  $13.0 \text{ cm s}^{-1}$  (in fact, using weekly data only 5% of the summer equatorward velocities are larger than  $13.0 \text{ cm s}^{-1}$ ).

[25] The seasonal cycle—estimated by least squares fitting of an annual harmonic—of the meridional geostrophic currents has maximum amplitude near the coast south of 35°S, with maximum equatorward values occurring during February and March for both satellite altimetry and in the model (Figures 9b and 9c). In this region the maximum amplitude ( $\sim 5 \text{ m s}^{-1}$ ) of the wind is also observed (Figure 9a). In the northern part of the study region the

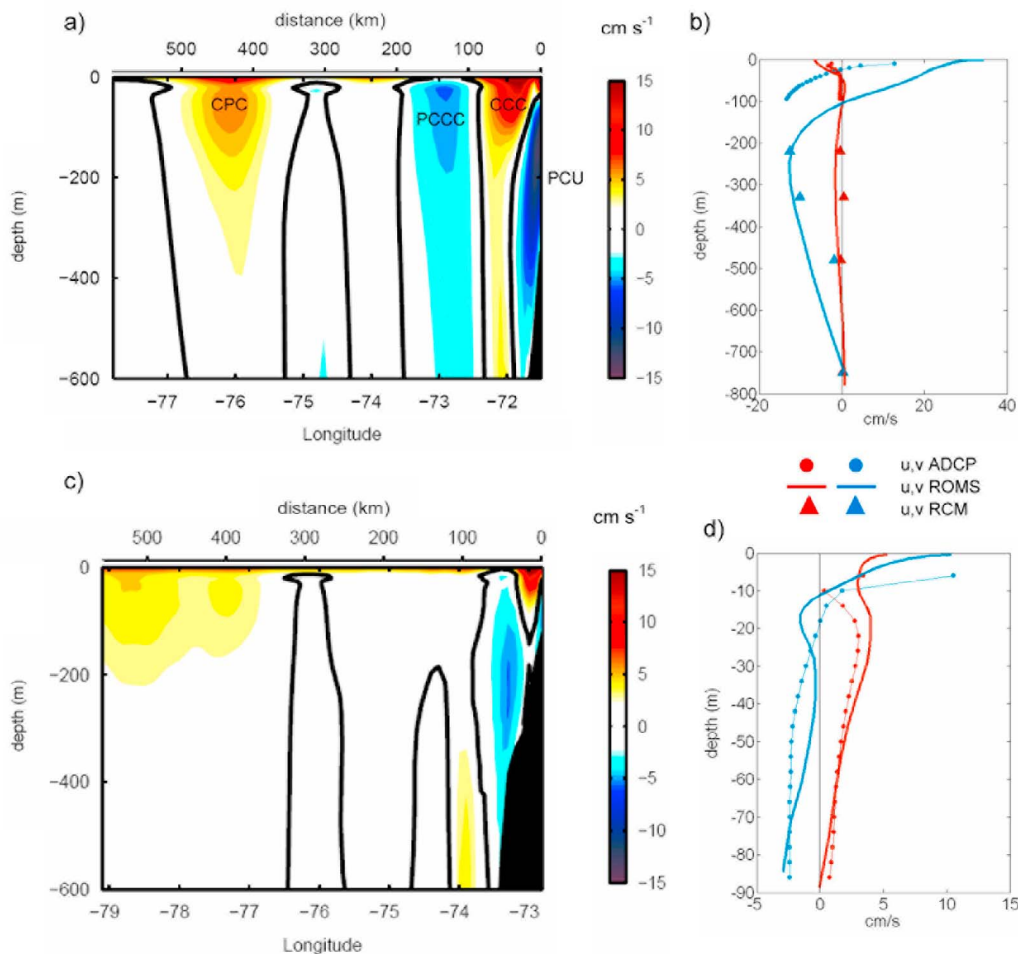


**Figure 6.** Mean vertical section of the simulated meridional currents at (a) 30°S and (c) 36°S. Mean profiles of the meridional (black) and zonal (gray) currents at the moorings (b) COSMOS and (d) Station 18.

annual cycle of the meridional geostrophic current is not significant (white regions); i.e., the correlation coefficients between the adjusted annual harmonic and the observed (or model) time series are not significantly different from zero (at the 95% level of confidence according to the *t-test*). On the other hand, the phase observed in the satellite and model geostrophic current (arrows in Figure 9) are similar. In both cases the phases suggest an offshore propagation of the meridional current. The large amplitude observed offshore north of Punta Lavapie ( $\sim 37^\circ\text{S}$ ) is directly related to the presence of the CTZ jet during spring and summer (cf. Figures 8a and 8b).

[26] Spectra for the wind stress and surface geostrophic currents were calculated based on the corresponding time series and then averaged inside a box of  $1^\circ$  of latitude and  $5^\circ$  of longitude starting with the valid data near the coast. The relative importance of the annual cycle of the wind stress and the meridional surface current from the model and altimetry increases with latitude (Figure 10). In fact, in the northern part of the domain (i.e., north of  $35^\circ\text{S}$ ), the spectral maxima for the surface geostrophic flow are near the semi-annual frequency, with no significant peaks at the annual frequency. The spectral maxima for this variable are near the semiannual frequency. In contrast, south of  $36^\circ\text{S}$  all the spectra are dominated by an annual peak.

### 3.3. Vertical Structure of the CTZ Jet

[27] In this section we present the vertical structure of the CTZ jet through vertical sections of the simulated meridional currents. Because the CTZ jet is fully developed during summer (DJF), only summer means at different latitudes are presented (Figure 11). The axis of the CTZ jet observed during summer clearly exhibits its westward displacement as the flow travels northward (see red arrows in Figure 11). The vertical extension of the CTZ jet increases at lower latitudes reaching values close to  $10\text{ cm s}^{-1}$  at about 200 m depth at  $30^\circ\text{S}$  and  $33^\circ\text{S}$ , transporting approximately  $3.2\text{ Sv}$ . This deepening may represent the process referred as “barotropization,” in which the jet separates from the coast at Punta Lavapie and undergoes baroclinic instability, deepening through the transformation of kinetic energy from vertically sheared flow into the vertical mean flow [Haney *et al.*, 2001].

[28] In Table 2 we quantify the meridional transports (Sv) for the four main alongshore flows off central Chile at four latitudes. We also estimate the *Humboldt* transport as the large scale equatorward flow between 200 and 600 km offshore and 600 m depth. Transport due to the simulated CTZ jet was calculated only for the summer season, when it is well developed. At  $30^\circ\text{S}$  and  $33^\circ\text{S}$  the transport of the CTZ



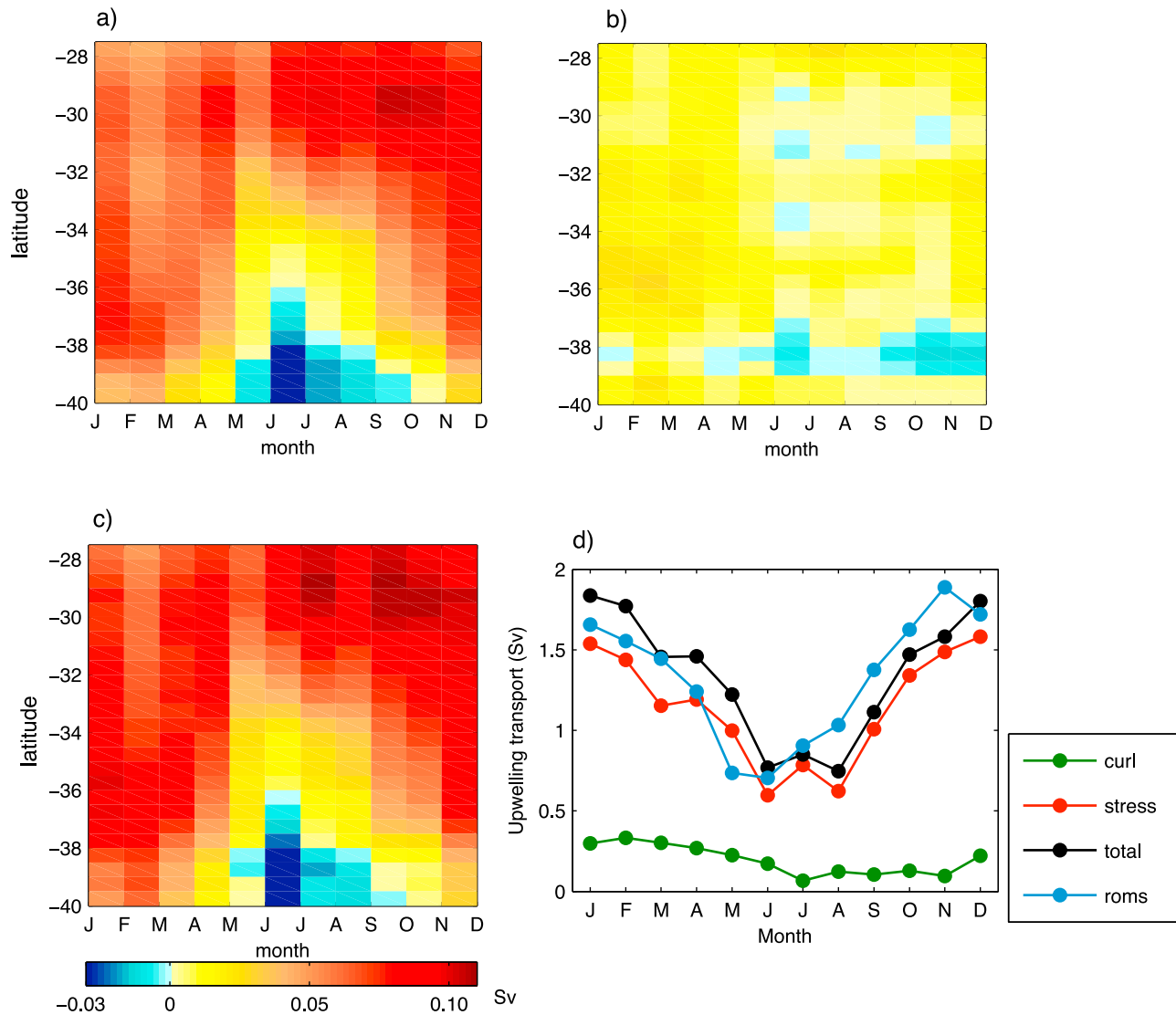


**Figure 7.** Contributions of the Ekman transport and Ekman pumping to the vertical transport near the coast (within the first 150 km offshore). (a) Seasonal vertical transport associated with Ekman transport, (b) seasonal vertical transport associated with Ekman pumping and (c) seasonal total wind induced vertical transport (Ekman transport + Ekman pumping). (d) Vertical transport (Sv) associated with Ekman transport (red), Ekman pumping (green), total wind induced vertical transport (Ekman transport + Ekman pumping, black) and simulated vertical velocities at 30 m depth (blue). Vertical velocities were integrated between 27°S and 40°S, and the first 150 km offshore.

jet during summer is a significant proportion (60–80%) of this *Humboldt* transport.

[29] Transport calculations for the other major flows off central Chile (Table 2) show that the CCC exhibits a distinct seasonal cycle in the southern part of the domain, being more intense during spring-summer and weaker in fall-winter. This seasonality is directly related to the upwelling dynamics [e.g., *Aiken et al.*, 2008]. The PCU shows more seasonality at 33°S and 36°S with higher values during spring-summer and summer-fall, respectively. At 39°S the PCU is considerably weaker and it is not present during spring. According to model results the PCCC does not show strong seasonality, but is very weak (velocities  $< 3 \text{ cm s}^{-1}$ ) during spring at 33°S.

### 3.4. The Role of Wind Stress Curl in the CTZ Jet Variability

[30] In the large scale context, the wind stress curl field (cf. Figure 2) suggests, through Sverdrup dynamics, a southward transport during spring and summer close to the coast (within the first 150 km) and northward transport offshore. Sverdrup transport estimated directly from the wind stress curl agrees well with the model meridional transport (Figure 12). Estimates of geostrophic transport based on hydrographic data from WOCE P06 line at 32°S have values of  $\sim 8 \text{ Sv}$  to 90°W [*Shaffer et al.*, 2004], which also agree well with our model meridional transports. However, even though the large scale Sverdrup transports are consistent

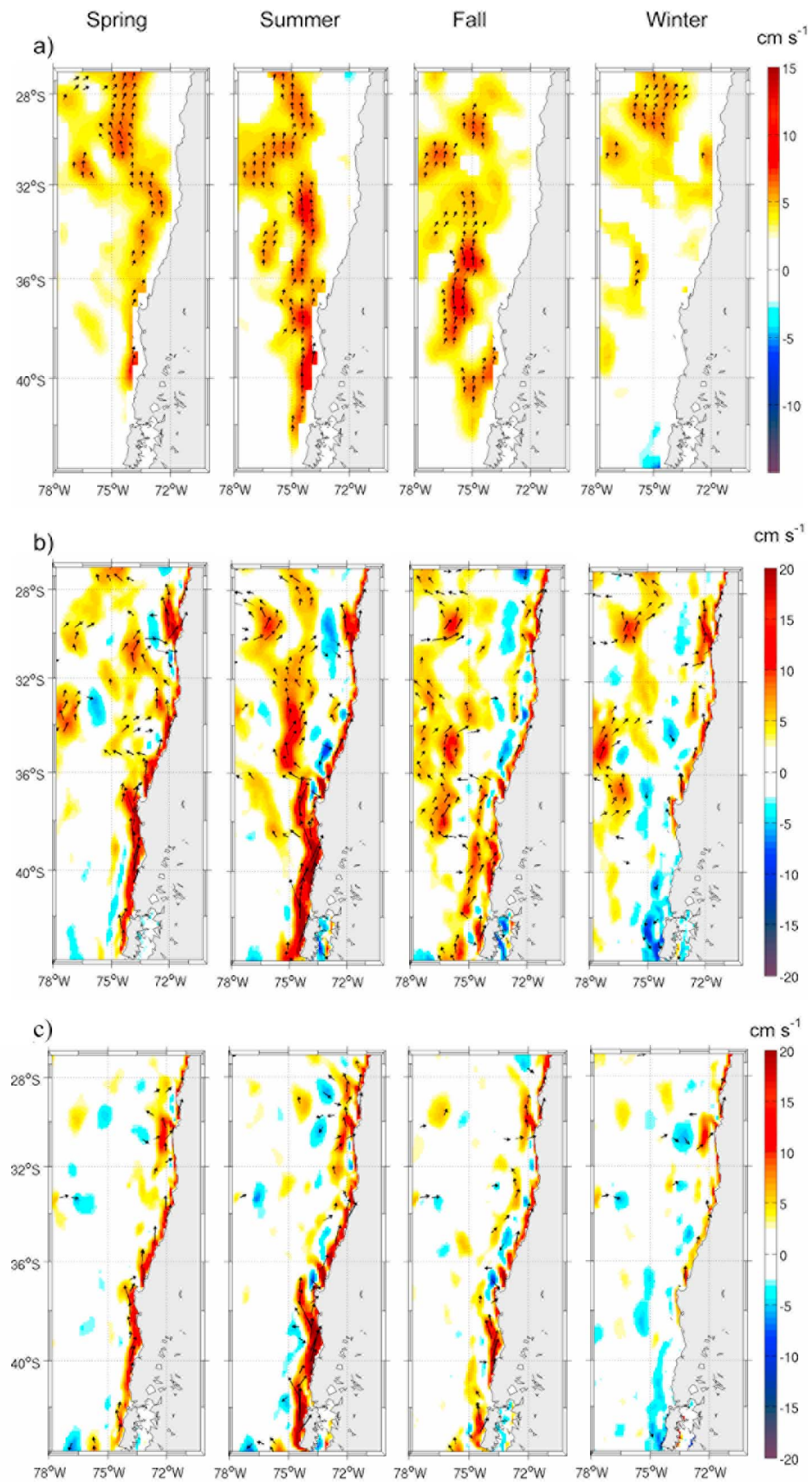
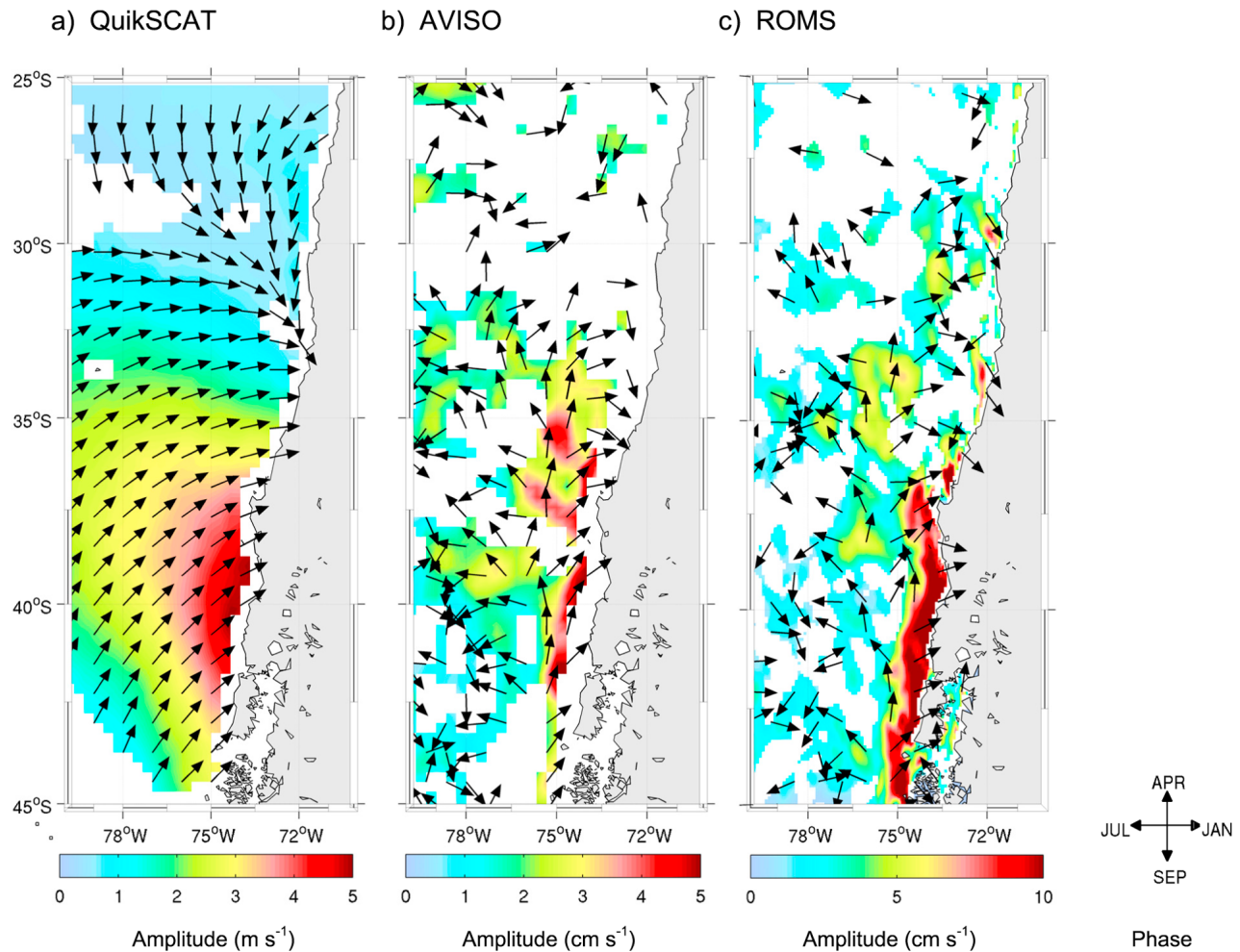


Figure 8



**Figure 9.** Amplitude (colors) and phase (vectors) of the annual cycle of the (a) meridional wind speed (QuikSCAT), (b) observed surface geostrophic meridional current (AVISO) and (c) model surface geostrophic meridional current. Results are plotted only when the adjusted annual harmonic of the wind and the observed (or model) time series of currents are significantly correlated using a *t*-test at the 95% level of confidence. White regions show not significant correlations.

with the model transports, the CTZ jet itself could be controlled by other dynamics that also involve the wind stress curl [Castelao and Barth, 2007].

[31] In order to evaluate the impact of the wind stress curl on the CTZ jet dynamics, we used a no-curl simulation (see methodology section). Comparing results between both simulations (i.e., the control and the no-curl runs) we found major differences only far from the coast (cf. Figures 8b and 8c). The CCC remains close to the coast and a poleward flow is developed during winter in the southern region, consistent with the wind stress there. The vertical structure of currents during summer at 30°S shows that both the CCC and the PCU are similar in both simulations (Figure 13). The poleward and the equatorward flows, associated with the PCCC and the CTZ jet respectively, in the control run, are

still present in the no-curl simulation; but their transports are reduced in magnitude. Notably, the equatorward jet-like flow observed offshore in the satellite data and in the control run, is not observed in the no-curl simulation. It is worth noting that boundary conditions may indirectly be imposing a flow by the use of climatological temperature and salinity fields. At 36°S, only the CCC is similar in both simulations. The PCU is weaker in the no curl simulation, but it still outcrops the surface as in the control run. The equatorward flow observed offshore of 100 km from the coast at 36°S is considerably weaker in the no curl simulation.

[32] These results show that the oceanic CTZ jet north of Punta Lavapie observed during spring and summer is not present in the no-curl simulation. In the satellite observations and in the control run the coastal jet observed south of

**Figure 8.** Seasonal climatology of the surface geostrophic meridional currents obtained from (a) a combination of mean surface geostrophic currents based on CARS temperature and salinity climatology (assuming a level of no motion at 1000 db) and geostrophic current anomalies derived from AVISO altimetry. (b) ROMS (control simulation) surface geostrophic meridional current and (c) ROMS (no-curl simulation) surface geostrophic meridional current. Vectors are shown only if the current speeds are higher than  $5 \text{ cm s}^{-1}$ .

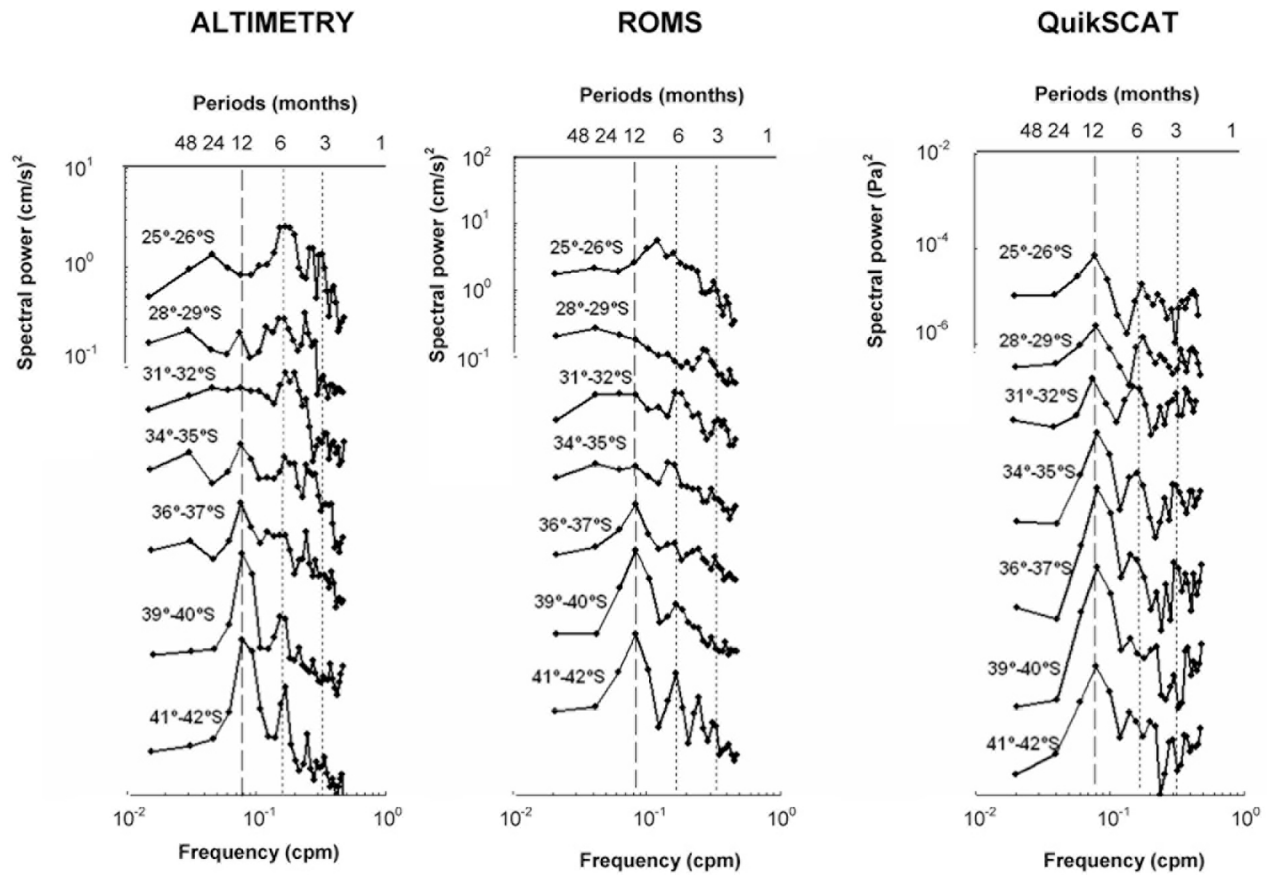


**Figure 10.** Spectra of the meridional geostrophic surface currents from altimetry data (AVISO) and model data (ROMS), and the spectra of the meridional wind stress from QuikSCAT data at different latitudes. The spectra inside a “box” of  $1^\circ$  latitude and the first  $5^\circ$  longitude offshore were averaged. The dashed line indicates the annual period and the dotted lines indicate the 6 and 3 months periods.

$37^\circ\text{S}$  separates from the coast at Punta Lavapie to form the CTZ jet. The separation of the coastal jet seems to be directly related to the wind stress curl. Indeed, the axis of the CTZ jet tends to follow the contour of zero wind stress curl from  $37^\circ\text{S}$  to  $32^\circ\text{S}$  (Figure 14). But farther north the CTZ is observed west of the zero wind stress curl during spring. According to the Sverdrup balance it is expected that the long-term mean position of the maximum surface current would be located near the contour of maximum anticyclonic curl. However, this contour is located far westward (more than 200 km) from the CTZ jet axis.

[33] On the other hand, the zero wind stress curl moves slightly offshore and extends southward from spring to summer, following the displacement of the axis of the atmospheric low-level jet present in the region from around  $38^\circ\text{S}$  to  $27^\circ\text{S}$  [Garreaud and Muñoz, 2005]. Note that the axis of the CTZ jet is observed just west of the zero wind stress curl in summer. The possible mechanism relating the wind stress curl and the CTZ jet are discussed below.

#### 4. Discussion

[34] Studies in the Pacific eastern boundary current systems provide examples of upwelling jets that separate from

the coast near capes to become oceanic jets [e.g., Barth and Smith, 1998; Barth et al., 2000]. Insights into this process were obtained by numerical experiments [Castelao and Barth, 2006, 2007; Mesias et al., 2003]. These model analyses showed that capes play a crucial role for separation of the coastal jet, and that the nonlinear terms in the equations that govern the flow are increased in the vicinity of a coastline perturbation or where the bottom topography orientation changes. In contrast, our two simulations (control and no-curl runs) used the same topography, but the CTZ jet was only observed when the wind stress curl was present in the surface forcing. This result shows that the wind stress curl plays a major role in the dynamics of the CTZ jet. Although the cape may be important for the separation of the coastal jet at Punta Lavapie, by itself it could not generate the CTZ jet observed off central Chile. Using an  $f$ -plane model, Castelao and Barth [2007], showed that the intensity of the wind stress is much less important than the position of the zero wind stress curl, which controls the location of the offshore jet. The mechanism proposed by those authors is that the spatial pattern of the wind stress curl generates a couplet of upwelling and downwelling regions (on each side of the zero wind stress curl line) that modify the density field and, thus, the position and intensity of the geostrophically

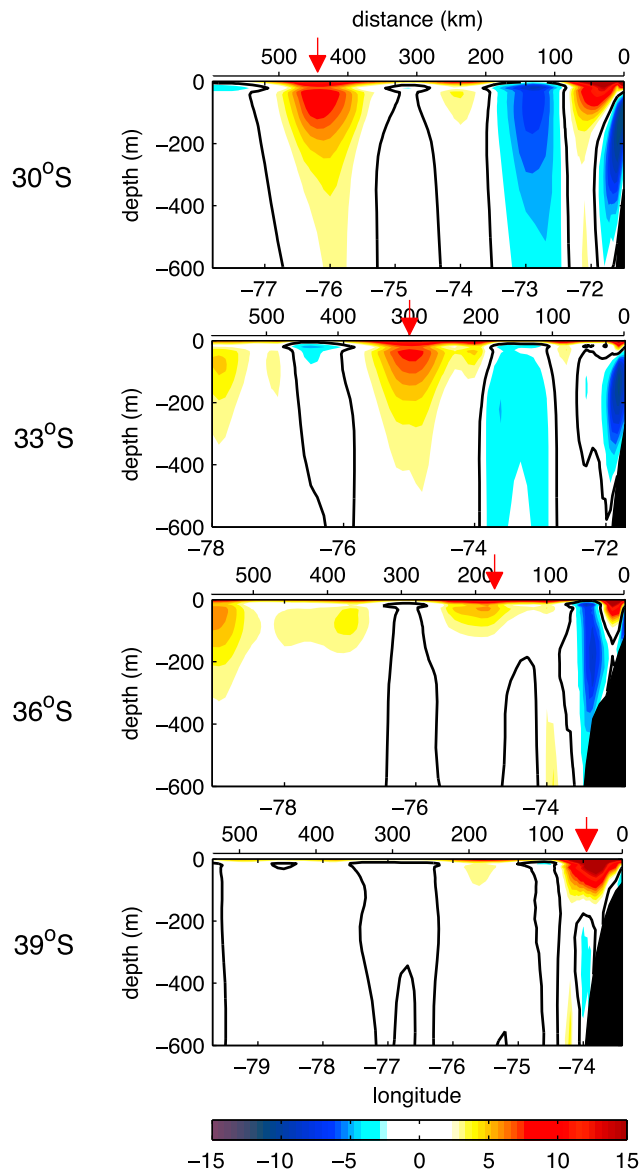


**Figure 11.** Vertical sections of the model meridional currents ( $\text{cm s}^{-1}$ ) at different latitudes during summer (DJF). The red arrows indicate the axis of the CTZ jet. Note that south of  $37^{\circ}\text{S}$  the CTZ jet cannot be separated from the CCC.

balanced jet. This process is consistent with our model observations, which find a region of cyclonic curl onshore (upwelling) and anticyclonic curl offshore (downwelling) of the CTZ jet. The jet follows (approximately) the zero wind stress curl. Hence, the seasonal variability of the CTZ jet is related to the seasonal variability of the Ekman pumping process superimposed on a large scale context dominated by the Sverdrup dynamics.

[35] Tracing these processes into the atmosphere, the positions of the zero wind stress curl and the CTZ jet correspond approximately to the climatological position of the core of the low-level atmospheric jet that is rooted at Punta Lavapie. This wind jet, in turn, is determined by the temperature gradient in the lower troposphere, which is maximum downstream of the major capes along the coast [Rahn

*et al.*, 2011]. Thus, Punta Lavapie may indirectly affect the location of the CTZ jet separation, by generating a recurrent atmospheric coastal wind jet during summer. The wind jet then impacts the upper-ocean circulation via the wind stress curl field.

[36] Major eastern boundary current systems are driven by predominant equatorward winds, which force coastal upwelling, equatorward surface flows and a poleward undercurrent [e.g., Hill *et al.*, 1998]. In this context, it is worth mentioning a brief comparison between the California and Humboldt Current System, particularly on the CTZ jet. The Coastal Transition Zone experiment conducted off northern California ( $\sim 39^{\circ}\text{N}$ ) provided evidences of a strong surface alongshore jet flowing equatorward [Brink and Cowles, 1991]. During spring and summer the model fields strongly support the concept of a meandering jet, which carries most of the surface transport in this period [Strub *et al.*, 1991]. The equatorward CTZ jet is narrow ( $50\text{--}75\text{ km}$ ) and exhibits its maximum values at the surface ( $>50\text{ cm s}^{-1}$ ), decreasing to velocities of  $10\text{ cm s}^{-1}$  about  $200\text{ m}$  deep. Its equatorward transport is  $\sim 4\text{ Sv}$  and it may be identified as the core of the California Current [Huyer *et al.*, 1991b]. The spatial pattern and the equatorward transport associated with the CTZ jet during spring and summer in the California Current agrees well with the CTZ jet described here off central Chile as a major component of the Humboldt Current. This jet transports about  $3\text{ Sv}$ , which is  $\sim 1\text{ Sv}$  smaller than its counterpart in the California Current System. Using satellite height fields Strub and James [2000] define a conceptual model of the seasonal evolution of the surface circulation in the California Current System. During spring and summer, an equatorward flow develops close to the coast ( $\sim 123^{\circ}\text{W}$ ), with an initial latitudinal structure that responds to the latitudinal distribution of the equatorward winds. This jet moves offshore from spring to fall to around  $130^{\circ}\text{W}$ , where the jet weakens and dissipates. The westward velocity propagation of the jet is consistent with the Rossby

**Table 2.** Seasonal Transport (Sv) of the Major Currents of the Chile-Peru Current System, Obtained Integrating to  $600\text{ m}$  Deep

	CCC	PCU	PCCC	Humboldt	CTZ Jet <sup>a</sup>
<b><math>30^{\circ}\text{S}</math></b>					
Fall	0.77	-1.06	-1.78	3.15	-
Winter	1.73	-0.86	-1.99	3.60	-
Spring	1.96	-0.87	-0.90	3.01	-
Summer	1.13	-0.81	-2.27	3.96	3.16
<b><math>33^{\circ}\text{S}</math></b>					
Fall	0.51	-0.81	-1.49	4.70	-
Winter	0.78	-0.61	-1.29	3.57	-
Spring	1.09	-0.70	-0.26	4.97	-
Summer	0.54	-0.73	-1.39	5.18	3.17
<b><math>36^{\circ}\text{S}</math></b>					
Fall	0.47	-0.68	-	3.75	-
Winter	0.39	-0.55	-	3.85	-
Spring	1.05	-0.43	-	3.44	-
Summer	0.47	-0.85	-	4.44	1.37
<b><math>39^{\circ}\text{S}</math></b>					
Fall	0.62	-0.34	-	1.86	-
Winter	0.36	-0.20	-	2.14	-
Spring	1.20	-	-	2.01	-
Summer	1.07 <sup>b</sup>	-0.17	-	1.54	1.07 <sup>b</sup>

<sup>a</sup>The transport of the CTZ jet is only estimated during summer when it is fully developed.

<sup>b</sup>South of  $37^{\circ}\text{S}$ , the CTZ jet cannot be separated from the CCC.

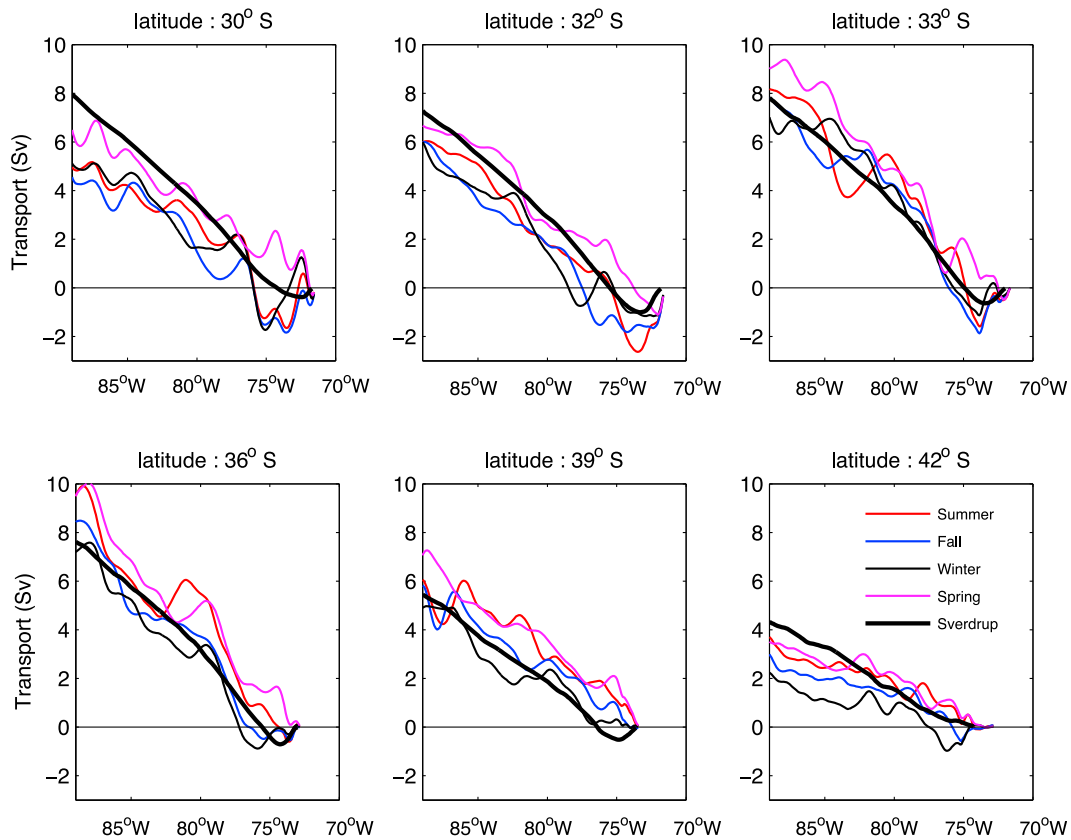


**Figure 12.** Seasonal surface transport (0–600 m depth) integrated westward along different latitudes from the Chilean coast based on model results. The thick black line shows the Sverdrup transport estimated directly from the annual mean wind stress curl (QuikSCAT data).

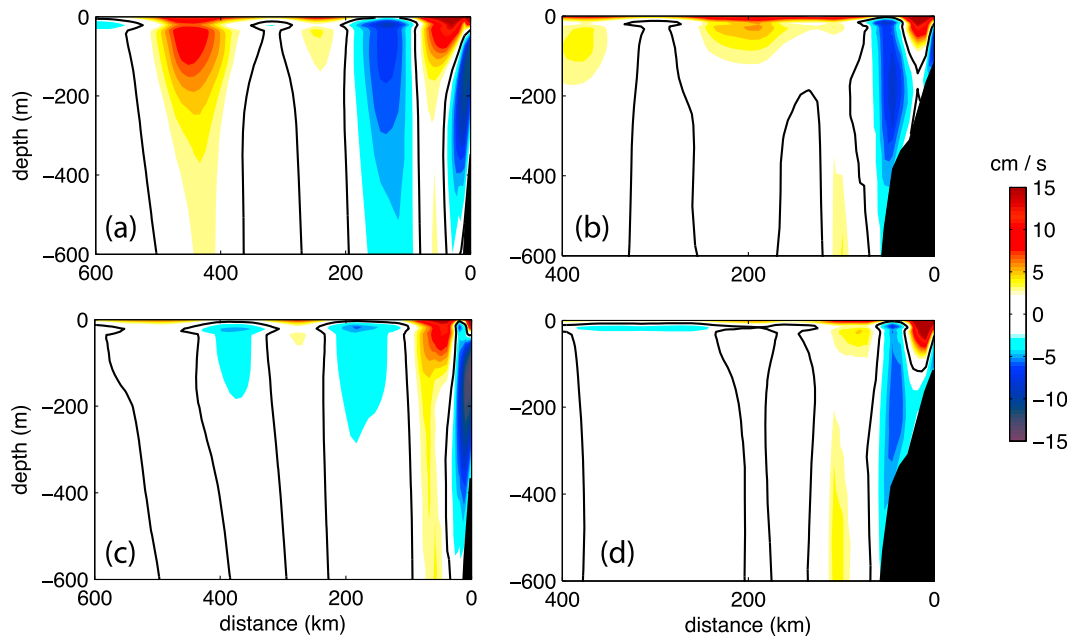


**Figure 13.** Vertical sections of the summer mean meridional flow at (a and c) 30°S and (b and d) 36°S obtained from the control (Figures 13a and 13b) and the no-curl (Figures 13c and 13d) simulations.

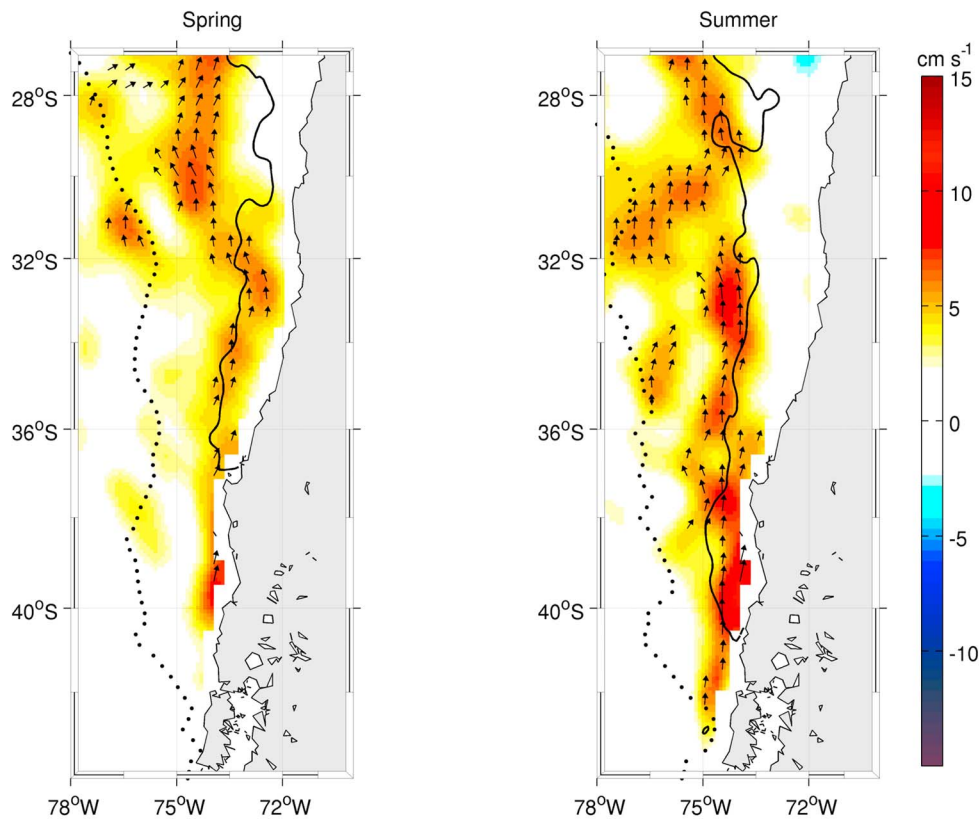


**Figure 14.** Spring and summer climatology of the observed surface geostrophic meridional currents from CARS 2006 plus AVISO (colors) as in Figure 8a. The continuous line indicates the zero wind stress curl and the dotted line indicates the position of the maximum values of the anticyclonic wind stress curl.

wave dynamics. A similar seasonal cycle is found in the Humboldt Current System. The jet develops during spring and summer, responding to the wind-forcing, and continuously moves offshore, becoming a more disorganized structure in winter. However, the CTZ jet of the Humboldt Current seems to be formed by the coastal jet separation observed at Punta Lavapie.

## 5. Conclusions

[37] In this work we have characterized the alongshore flows off central Chile, particularly the coastal transition zone jet and its seasonal variability, using geostrophic velocities derived from satellite altimetry and from simulations using the regional ocean model (ROMS). We perform two simulations that only differ in their surface wind-forcing. The standard case uses long-term monthly mean wind stress from QuikSCAT and the second uses a wind stress field without curl (the “no curl” simulation). Both the observed and model geostrophic surface currents show a well defined equatorward flow with a jet like-structure which develops during spring and summer and moves westward as the year progresses. In fall the jet is located offshore and becomes weaker. In contrast, during winter the flow is in general much weaker and a poleward flow is observed close to the coast in the southern region. There the amplitude of the annual cycle of the geostrophic current is larger, consistent

with the maximum amplitude of the annual cycle of the wind stress.

[38] The model is able to reproduce the major features observed off central Chile, such as a coastal surface equatorward jet, a poleward undercurrent with a core over the upper slope, and a countercurrent located westward of the coastal jet. In addition, the model reproduces the coastal jet separation at Punta Lavapie ( $\sim 37^\circ\text{S}$ ) during the summer to become the offshore CTZ jet, which is also observed by altimetry data. This striking feature is not replicated by the surface geostrophic currents in the no-curl simulation, so the CTZ is not present during the spring and summer off central Chile. Although Sverdrup transport was similar to the model transport in a large scale context, the CTZ jet is not located where the positive wind stress curl is maximum (Sverdrup transport is maximum), which is found farther offshore. In contrast, the position of the CTZ jet seems to be related to the zero wind stress curl contour, which corresponds to the climatological location of the axis of the low-level atmospheric jet. Thus, both the oceanic and the atmospheric jets are aligned about the same axis. These results illustrate the importance of the offshore upwelling/downwelling associated with the Ekman pumping, which tilts the isopycnals upward, creating a northward flow through thermal wind balance. Our results show that the cape could be important for separation of the coastal jet at Punta Lavapie, but is not enough to generate (by itself) the CTZ jet observed off central Chile. Indeed, the presence of Punta Lavapie and the

abrupt change in coastline orientation downstream of it seem fundamental in producing a recurrent and intense atmospheric low-level coastal wind jet in this area, which in turn produces the marked change in wind stress curl near the coast and offshore.

[39] In this work we have focused on the seasonal variability of the alongshore currents, without considering intraseasonal fluctuations, the large, well-documented interannual variability, and climate change. South of 20°S intraseasonal wind fluctuations are well correlated with wind fluctuations in the equatorial Pacific, associated with the Madden-Julian Oscillation [Hormazabal *et al.*, 2002]. Although intraseasonal fluctuations in the wind stress curl itself have not been specifically addressed, it is plausible that these exist, which could introduce intraseasonal variability in the CTZ jet. The interannual variability related to the El Niño-Southern Oscillation (ENSO) cycle may directly modulate the CTZ jet due to changes in the wind stress related, in turn, to disturbances in the South Pacific subtropical anticyclone, or indirectly due to the extra-tropical interannual oceanic Rossby wave that is forced by the ENSO in the eastern South Pacific [Vega *et al.*, 2003]. On the other hand, regional climate simulations for future scenarios of increased warming have indicated an increase in southerly winds during spring and summer off western subtropical South America, expanding the upwelling-favorable regime [Garreaud and Falvey, 2009]. If the wind stress curl pattern is changed, the equatorward CTZ jet would presumably be influenced. The interannual variability of the CTZ jet as well its long-term change is under consideration as a future work in order to document more completely the dynamics of this flow.

[40] **Acknowledgments.** This study was supported by FONDECYT 1090791. CA was supported by the MECESUP 0310 Ph.D. grant. She also benefited from technical visits to the Laboratoire d'Etudes en Géophysique et Océanographie Spatiales (LEGOS, Toulouse, France), with travel support from ECOS-CONICYT, and to the College of Oceanic and Atmospheric Sciences, Oregon State University (Corvallis, Oregon, United States), with travel support from Vicerectoria de Asuntos Academicos (VAA) and Facultad de Ciencias Físicas y Matemáticas (FCFM), Universidad de Chile, and SACC-IAI CRN 061. We thank an anonymous reviewer and Alexis Chaigneau for their positive and constructive comments and suggestions that improved this manuscript.

## References

- Aiken, C., M. Castillo, and S. Navarrete (2008), A simulation of the Chilean Coastal Current and associated topographic upwelling near Valparaíso, Chile, *Cont. Shelf Res.*, **28**, 2371–2381, doi:10.1016/j.csr.2008.05.006.
- Antonov, J., R. Locarnini, T. Boyer, A. Mishonov, and H. Garcia (2006), *World Ocean Atlas 2005*, vol. 2, *Salinity*, NOAA Atlas NESDIS, vol. 62, edited by S. Levitus, 182 pp., NOAA, Silver Spring, Md.
- Bakun, A., and C. S. Nelson (1991), The seasonal cycle of wind stress curl in sub-tropical eastern boundary current region, *J. Phys. Oceanogr.*, **21**, 1815–1834, doi:10.1175/1520-0485(1991)021<1815:TSCOWS>2.0.CO;2.
- Barth, J., and R. Smith (1998), Separation of a coastal upwelling jet at Cape Blanco, Oregon, USA, *S. Afr. J. Mar. Sci.*, **19**, 5–14, doi:10.2989/025776198784126674.
- Barth, J., S. Pierce, and R. Smith (2000), A separating coastal upwelling jet at Cape Blanco, Oregon and its connection to the California Current System, *Deep Sea Res. Part II*, **47**, 783–810, doi:10.1016/S0967-0645(99)00127-7.
- Batteen, M., C. Hu, J. Bacon, and C. Nelson (1995), A numerical study of the effects on wind forcing on the Chile Current System, *J. Oceanogr.*, **51**, 585–614, doi:10.1007/BF02270526.
- Brink, K. H., and T. J. Cowles (1991), The Coastal Transition Zone Program, *J. Geophys. Res.*, **96**(C8), 14,637–14,647, doi:10.1029/91JC01206.
- Capet, X., P. Marchesiello, and J. McWilliams (2004), Upwelling response to coastal wind profiles, *Geophys. Res. Lett.*, **31**, L13311, doi:10.1029/2004GL020123.
- Castelao, R., and J. Barth (2006), The relative importance of wind strength and along-shelf bathymetric variations on the separation of a coastal upwelling jet, *J. Phys. Oceanogr.*, **36**, 412–425, doi:10.1175/JPO2867.1.
- Castelao, R., and J. Barth (2007), The role of wind stress curl in jet separation at a cape, *J. Phys. Oceanogr.*, **37**, 2652–2671, doi:10.1175/2007JPO3679.1.
- Chaigneau, A., and O. Pizarro (2005), Mean surface circulation and mesoscale turbulent flow characteristics in the eastern South Pacific from satellite tracked drifters, *J. Geophys. Res.*, **110**, C05014, doi:10.1029/2004JC002628.
- da Silva, A. M., C. C. Young, and S. Levitus (Eds.) (1994), *Atlas of Surface Marine Data 1994*, vol. 1, *Algorithms and Procedures*, NOAA Atlas NESDIS, vol. 6, 83 pp., NOAA, Silver Spring, Md.
- Fuenzalida, H. (1971), *Climatología de Chile*, 72 pp., Dep. de Geofis., Univ. de Chile, Santiago.
- Fuenzalida, R., W. Schneider, J. Garcés-Vargas, and L. Barvo (2008), Satellite altimetry data reveal jet-like dynamics of the Humboldt Current, *J. Geophys. Res.*, **113**, C07043, doi:10.1029/2007JC004684.
- Garreaud, R. D., and M. Falvey (2009), The coastal winds off western subtropical South America in future climates scenarios, *Int. J. Climatol.*, **29**, 543–554, doi:10.1002/joc.1716.
- Garreaud, R. D., and R. C. Muñoz (2005), The low level jet off the west coast of subtropical South America: Structure and variability, *Mon. Weather Rev.*, **133**, 2246–2261, doi:10.1175/MWR2972.1.
- Haney, R., R. Hale, and D. Dietrich (2001), Offshore propagation of eddy kinetic energy in the California Current, *J. Geophys. Res.*, **106**(C6), 11,709–11,717, doi:10.1029/2000JC000433.
- Hill, A. E., B. Hickey, F. Shillington, P. T. Strub, K. H. Brink, E. Barton, and A. Thomas (1998), Eastern boundary currents: A pan-regional review, in *The Sea*, vol. 11, *The Global Coastal Ocean: Regional Studies and Syntheses*, edited by A. R. Robinson and K. H. Brink, pp. 29–68, John Wiley, Hoboken, N. J.
- Hormazabal, S., G. Shaffer, and O. Pizarro (2002), Tropical Pacific control of intraseasonal oscillations off Chile by way of oceanic and atmospheric pathways, *Geophys. Res. Lett.*, **29**(6), 1081, doi:10.1029/2001GL013481.
- Hormazabal, S., G. Shaffer, and O. Leth (2004), Coastal transition zone off Chile, *J. Geophys. Res.*, **109**, C01021, doi:10.1029/2003JC001956.
- Huyer, A., M. Knoll, T. Paluszkiwicz, and R. Smith (1991a), The Perú Undercurrent: A study in variability, *Deep Sea Res.*, **38**, 247–279.
- Huyer, A., M. Kosro, J. Feischbein, S. Ramp, T. Stanton, L. Washburn, F. Chavez, T. Cowles, S. Pierce, and R. Smith (1991b), Currents and water masses of the coastal transition zone off northern California, June to August 1988, *J. Geophys. Res.*, **96**, 14,809–14,831, doi:10.1029/91JC00641.
- Large, W., J. McWilliams, and S. Doney (1994), Oceanic vertical mixing: A review and a model with a nonlocal boundary layer parameterizations, *Rev. Geophys.*, **32**, 363–403, doi:10.1029/94RG01872.
- Letelier, J., O. Pizarro, and S. Nuñez (2009), Seasonal variability of coastal upwelling and the upwelling front off central Chile, *J. Geophys. Res.*, **114**, C12009, doi:10.1029/2008JC005171.
- Leth, O., and J. Middleton (2004), A mechanism for enhanced upwelling off Central Chile: Eddy advection, *J. Geophys. Res.*, **109**, C12020, doi:10.1029/2003JC002129.
- Leth, O., and G. Shaffer (2001), A numerical study of the seasonal variability in the circulation off central Chile, *J. Geophys. Res.*, **106**, 22,229–22,248, doi:10.1029/2000JC000627.
- Locarnini, R., A. Mishonov, J. Antonov, T. Boyer, and H. Garcia (2006), *World Ocean Atlas 2005*, vol. 1, *Temperature*, NOAA Atlas NESDIS, vol. 61, edited by S. Levitus, 182 pp., NOAA, Silver Spring, Md.
- Marchesiello, P., J. McWilliams, and A. Shchepetkin (2001), Open boundary conditions for long-term integration of regional oceanic models, *Ocean Modell.*, **3**, 1–20, doi:10.1016/S1463-5003(00)00013-5.
- McCreary, J. P., and S. Y. Chao (1985), Three-dimensional shelf circulation along an eastern ocean boundary, *J. Mar. Res.*, **43**, 13–36, doi:10.1357/002224085788437316.
- Mesias, J., R. Matano, and P. T. Strub (2001), A numerical study of the upwelling circulation off central Chile, *J. Geophys. Res.*, **106**, 19,611–19,623, doi:10.1029/2000JC000649.
- Mesias, J., R. Matano, and P. T. Strub (2003), Dynamical analysis of the upwelling circulation off central Chile, *J. Geophys. Res.*, **108**(C3), 3085, doi:10.1029/2001JC001135.
- Muñoz, R., and R. Garreaud (2005), Dynamics of the low level jet off the west coast of subtropical South America, *Mon. Weather Rev.*, **133**, 3661–3677, doi:10.1175/MWR3074.1.
- Penven, P., V. Echevin, J. Pasapera, F. Colas, and J. Tam (2005), Average circulation, seasonal cycle and mesoscale dynamics of the Perú Current



- System: A modeling approach, *J. Geophys. Res.*, *110*, C10021, doi:10.1029/2005JC002945.
- Pizarro O., S. Hormazábal, A. González and E. Yañez (1994), Variabilidad del viento, nivel del mar y temperatura en la costa norte de Chile, *Invest. Mar.*, *22*, 85–101.
- Rahn, D., R. Garreaud, and J. Rutllant (2011), The low-level atmospheric circulation near Tongoy Bay–Point Lengua de Vaca (Chilean coast, 30°S), *Mon. Weather Rev.*, *139*, 3628–3647.
- Ridgway, K., J. Dunn, and J. Wilkin (2002), Ocean interpolation by four-dimensional weighted least squares—Application to the waters around Australasia, *J. Atmos. Oceanic Technol.*, *19*, 1357–1375, doi:10.1175/1520-0426(2002)019<1357:OIBFDW>2.0.CO;2.
- Saavedra, N., and A. Foppiano (1992), Monthly mean pressure model for Chile, *Int. J. Climatol.*, *12*, 469–480, doi:10.1002/joc.3370120505.
- Shaffer, G., O. Pizarro, L. Djurfeldt, S. Salinas, and J. Rutllant (1997), Circulation and low-frequency variability near the Chile coast: Remotely forced fluctuations during the 1991–1992 El Niño, *J. Phys. Oceanogr.*, *27*, 217–235, doi:10.1175/1520-0485(1997)027<0217:CALFVN>2.0.CO;2.
- Shaffer, G., S. Hormazábal, O. Pizarro, L. Djurfeldt, and S. Salinas (1999), Seasonal and interannual variability of currents and temperature over the slope off central Chile, *J. Geophys. Res.*, *104*, 29,951–29,961, doi:10.1029/1999JC900253.
- Shaffer, G., S. Hormazábal, O. Pizarro, and M. Ramos (2004), Circulation and variability in the Chile Basin, *Deep Sea Res. Part I*, *51*, 1367–1386, doi:10.1016/j.dsr.2004.05.006.
- Shchepetkin, A., and J. McWilliams (2005), The regional oceanic modeling system (ROMS): A split-explicit, free-surface, topography-following-coordinate oceanic model, *Ocean Modell.*, *9*, 347–404, doi:10.1016/j.ocemod.2004.08.002.
- Silva, N., and S. Neshyba (1979), On the southernmost extension of the Perú-Chile Undercurrent, *Deep Sea Res.*, *26*, 1387–1393, doi:10.1016/0198-0149(79)90006-2.
- Smith, W., and D. Sandwell (1997), Global seafloor topography from satellite altimetry and ship depth soundings, *Science*, *277*, 1956–1962, doi:10.1126/science.277.5334.1956.
- Stewart, R. (2008), *Introduction to Physical Oceanography*, Dep. of Oceanogr., Tex. A&M Univ., College Station, Tex.
- Strub, P. T., and C. James (2000), Altimeter-derived variability of surface velocities in the California Current System: Part 2. Seasonal circulation and eddy statistics, *Deep Sea Res. Part II*, *47*, 831–870, doi:10.1016/S0967-0645(99)00129-0.
- Strub, P. T., P. Kosro, A. Huyer, and C. Collaborators (1991), The nature of the cold filaments in the California Current System, *J. Geophys. Res.*, *96*(C8), 14,743–14,768, doi:10.1029/91JC01024.
- Strub, P. T., M. Mesias, and C. James (1995), Altimeter observations of the Perú-Chile Countercurrent, *Geophys. Res. Lett.*, *22*, 211–214, doi:10.1029/94GL02807.
- Strub, P. T., V. Montecino, J. Rutllant, and S. Salinas (1998), Coastal ocean circulation off western south America, in *The Sea*, vol. 11, *The Global Coastal Ocean: Regional Studies and Syntheses*, edited by A. R. Robinson and K. H. Brink, pp. 273–314, John Wiley, Hoboken, N. J.
- Vega, A., Y. du-Penhoat, B. Dewitte, and O. Pizarro (2003), Equatorial forcing of interannual Rossby waves in the eastern South Pacific, *Geophys. Res. Lett.*, *30*(5), 1197, doi:10.1029/2002GL015886.
- C. Aguirre and R. Garreaud, Department of Geophysics, University of Chile, Blanco Encalada 2002, Casilla 2777, Santiago, Chile. (catalina@dgf.uchile.cl)
- J. A. Barth and P. T. Strub, College of Oceanic and Atmospheric Sciences, Oregon State University, 104 COAS Administration Bldg., Corvallis, OR 97331-5503, USA.
- Ó. Pizarro, Department of Geophysics, University of Concepcion, Avda. Esteban Iturra s/n, Barrio Universitario, Casilla 160-C, Concepcion, Chile.